Journal of Applied Science, Innovation & Technology (JASIT)

Research Article

https://prakritimitrango.com

Fabrication of iron nanoparticles by reusing an iron waste and their application as efficient adsorbents to remove crystal violet dye from water

Shalu Rawat*, Jiwan Singh
Department of Environmental Science, Babasaheb Bhimrao Ambedkar University, Lucknow-226025, Uttar Pradesh, India
ARTICLE INFOR: *Received: 13, November, 2022, Revised: 23, November, 2022, Accepted: 24, November, 2022*
CORRESPONDING AUTHOR: shalurawat200@gmail.com (S. Rawat), Tel: +91-9807461701

Abstract
The present study reports an easy conversion of waste iron rust into nanosized iron adsorbents. These iron nanoparticles were applied for the eradication of Crystal violet (CV) by the adsorption method from aqueous solution. Both the synthesised nanoparticles (IRNPs@Pl and IRNPs@Ja) had different shapes and sizes as shown by scanning electron microscope (SEM), their elemental composition mainly comprised of "Fe", "O", "C" and "Cl" as per the energy dispersive X-ray spectroscopy (EDS). By using Fourier transform infrared spectroscopy (FTIR), many functional groups on the surface of nanoparticles were examined, revealing a complex surface chemistry. The XRD analysis showed that the nanoparticles were amorphous in nature. The synthesised adsorbents (Iron nanoparticles) were found efficient for dye adsorption. The highest value of adsorption percentage was found to be 85.50 % and 89.91 % using IRNPs@Pl and IRNPs@Ja, respectively. The adsorption data of CV using IRNPs@Pl fitted best with Langmuir adsorption isotherm while using IRNPs@Ja the adsorption data fitted best with Temkin isotherm. However, pseudo-second-order kinetics was followed best using both the nanoparticles.
Keywords: Iron nanoparticles; crystal violet dye; adsorption; isotherm; kinetics

1. Introduction

Nanotechnology has been proved to be successful nowadays in several fields (Khan et al., 2021). It is proving itself highly efficient in environmental remediation also. Several researches has been done upon the utilization of different type of nanomaterials for the remediation of air, water and soil pollution (Linley and Thomson 2021; Qian et al., 2020; Sharma et al., 2018). Nanoparticles have extremely small size and higher size to surface area ratio which provide them higher reactivity, and they possess some unique characteristic unlike their bulk materials (Das et al., 2019; Zhang et al., 2019). Due to their unique qualities the use of nanoparticles is increasing day by day. Different type of nanomaterial like carbon based nanomaterials: activated carbon (Nazir et al., 2021), carbon nanotubes, graphene (Wang et al., 2019), metallic nanoparticles: iron nanoparticles (Pasinszki and Krebsz, 2020), copper nanoparticles (Khani et al., 2018), silver nanoparticles (Parmar et al., 2019), gold nanoparticles (Mishra et al., 2020) and metal oxide nanoparticles: copper oxide nanoparticles (Akintelu et al., 2020), iron oxide nanoparticles (Leonel et al., 2021) zinc oxide nanoparticles (Kumar et al., 2019), titanium oxide nanoparticles (Abdulhameed et al., 2019), have been most commonly studied to treat waste water.

Iron nanoparticles are among the most frequently applied metallic nanoparticles (Hao et al., 2021). Zerovalent iron and iron oxides both types are reported to be effective for the adsorption, catalysis, and antimicrobial activity (Kaur et al., 2021; Chatterjee et al., 2020). Iron nanoparticles can be easily synthesised by green chemical route using the extract of plants as an eco-friendly reducing agent. This method of synthesis is facile, harmless for environment and economically efficient (Elgarahy et al. 2021; Xiao et al., 2020). In this study, we have reported fabrication of iron nanoparticles using iron extracted from iron rust, thus recycling the waste iron rust with no economic importance into a valuable product. The adsorption of CV dye was achieved using synthesized nanoparticles. Furthermore, this study also reports effects of different operational parameters on the adsorption efficiency.

2. Materials and methods

2.1. Chemicals and reagents

The entire inventory of analytical-grade chemicals and reagents used in this project was provided by Thermo Fisher. These chemicals and reagents were utilized without purifying further.

2.2. Synthesis of adsorbents

Iron nanoparticles utilized in this study were synthesised as described in our previously reported work (Rawat and Singh, 2023). Briefly, the iron extraction was done by leaching of 1g rust with 10 mL HCl (3M). The obtained leachate containing dissolved iron was filtered and diluted 50%. Then aqueous extract of dried leaves of *Jatropha* and *Plumeria* was added in the leachate drop by drop separately. The extraction of dried *Plumeria* and *Jatropha* leaves was done for the synthesis of nanoparticles by following the method of Rawat and Singh (2021). The addition of leaf extract in leachate was accompanied with strong continuous stirring and addition of NaOH solution was also done to raise the pH of reaction mixture to 6. A sudden change in colour of leachate to intense black was noticed upon addition of extract which represents the reduction of iron into zerovalent iron nanoparticles. Through centrifugation, the synthesised nanoparticles were washed and removed from the suspension. Distilled water was utilised prior to the use of ethanol to wash the nanoparticles. Thereafter, the nanoparticles were dried and grounded into fine powder and stored in an air tight tube. Iron nanoparticles synthesised using

Jatropha was termed as IRNPs@Ja and those synthesised using *Plumeria* were termed as IRNPs@Pl, both the nanoparticles were used for the adsorption of CV dye.

2.3. Characterizations of the adsorbents

Synthesized both adsorbents were analysed by SEM and EDS (Model: JSM 4490, JEOL, Japan) to investigate the morphology and elemental composition, respectively. Utilizing FTIR (Model: NICOLET 6700, Thermo Fischer Scientific, USA), surface functional groups of the nanoparticles were analysed using XRD (Model: D8 Advance Eco, Make: Bruker, Germany) to determine the crystalline nature of adsorbents. The zero point charge (pH_{ZPC}) of the adsorbents was also identified using the method of pH drift as discussed in the study of Shukla et al. (2020). The pH_{ZPC} is a significant analysis for the adsorbents, it determines the behaviour of adsorbents at different pH values. The surface of adsorbent does not carry any charge at pH equals to the value of pH_{ZPC} (Bhan and Singh, 2022) and below it adsorbent is positively charged, whereas, at pH above pH_{ZPC} the adsorbent surface remains negatively charged (Mashkoor and Nasar, 2020).

2.4. Adsorption of CV dye

The test to determine the adsorption efficiency of the synthesised adsorbents was employed over the aqueous solution of CV dye. Erlenmeyer flasks of 250 mL capacity were brought in use to perform all adsorption experiments. In a flask, 10 mg/L dye solution (50 mL) and a known concentration of adsorbent were taken, then the flask was shook for a definite time period at neutral pH and 25 ˚C after which separation of adsorbent was done from the dye solution. UV-Visible spectrophotometer (117, Systronics) was used to determine the remaining dye concentration at 580 nm. Adsorption of CV was optimized by altering the adsorbent quantity, concentration of adsorbate, adsorption time (from 0 to 300 min), pH 2 to 10 and temperature 25 to 55 ˚C. Adsorption % and adsorption capacity q_t (mg/g) were determined by the use of eq. (1) and (2).

$$Adsorption\ \% = \frac{C_0 - C_t}{C_0} \times 100 \qquad (1)$$

$$q_t\ (mg/g) = (C_0 - C_t)\frac{V}{m} \qquad (2)$$

Where V is the adsorbate volume (L) and m is the adsorbent mass employed in the study (g/L), C_0 and C_t are the respective CV concentrations (mg/L), prior and post adsorption.

2.5. Adsorption isotherms, kinetics and thermodynamic

Three adsorption isotherms were applied for the analysis of CV adsorption namely Langmuir, Freundlich and Temkin adsorption isotherm to analyse adsorption data. The linear equations for the isotherms are given in Table 1. Degradation data was also studied by the application of adsorption kinetics, intraparticle diffusion model and thermodynamics. Linear equations for these models have been provided in the Table 1 (Badeenezhad et al., 2019; Singh et al., 2016; Chowdhury et al., 2021; Saruchi et al., 2019).

Table 1. Adsorption isotherm, kinetics and thermodynamics models used to analyse the adsorption data of CV in this work

Models studied	Used linear equations	Parameters
Langmuir Isotherm	$\frac{C_e}{q_e} = \frac{1}{Q_0 b} + \frac{C_e}{Q_0}$	**Q_0** = maximum adsorption capacity, mg/g, **b** (L/mg) = adsorption rate **R_L** = dimensionless factor= $R_L = \frac{1}{(1+bC_0)}$
Freundlich Isotherm	$lnq_e = lnK_F + \left(\frac{1}{n}\right) lnC_e$	**K_F** (mg/g (L/mg)$^{1/n}$) = Freundlich constant, denotes adsorption capacity (mg/g (L/mg)$^{1/n}$) **n** = Freundlich constant
Temkin Isotherm	$q_e = BlnK_T + BlnC_e$	**B** = Temkin isotherm constant **K_T**= Temkin isotherm constant
Pseudo-First-order	$Log\ (q_e - q_t) = logq_e - \left(\frac{k_1}{2.303}\right) t$	**k_1** (min^{-1}) = pseudo-first-order kinetic constant
Pseudo-second-order	$\frac{t}{q_t} = \frac{1}{(K_2 q_e^2)} + \left(\frac{1}{q_e}\right) t$	**k_2** (g/(mg min)) = pseudo-first-order kinetic constant
Intraparticle diffusion models	$q_t = k_i t^{1/2} + C$	**k_i** (i (mg/g min$^{1/2}$) = intraparticle diffusion constant
Thermodynamics	$K_c = \frac{q_e}{C_e}$ $lnK_c = \frac{\Delta S°}{R} - \frac{\Delta H°}{RT}$ $\Delta G° = -RTlnK_c$	ΔH˚(kJ/mol) = enthalpy change ΔS˚ (kJ/mol K) = entropy change ΔG˚(kJ/mol) = Gibbs free energy change

"Where q_e and C_e stand for equilibrium adsorption capacity and dye concentration, respectively, t stands for time, R stands for the universal gas constant (8.314 J/mol K), and T stands for absolute temperature (K)."

2.6. Regeneration of the adsorbents

IRNPs@Ja and IRNPs@Pl after adsorption of CV were separated from dye solution and then they were dispersed in

distilled water for 2 h and then removed, dried overnight and reused in second cycle for adsorption of CV. In similar way, the adsorbents were utilized for five times.

3. Results and discussion

3.1. Characterization of adsorbents

SEM analysis of the adsorbents showed irregular shaped particles that were clumped together and no separate particle was recognised (Fig. 1a and 1b). After adsorption of CV, the size of particles increased and separate particles of different shapes and sizes were visible (Fig. 1c and 1d).

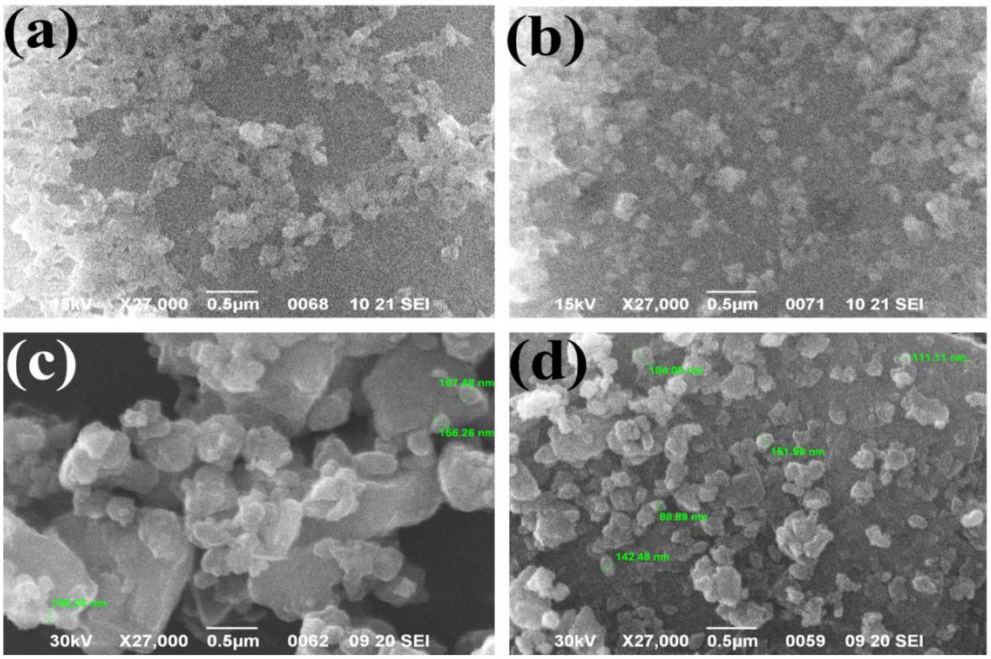

Fig. 1 SEM image of a) IRNPs@Pl and b) IRNPs@Ja before adsorption and c) IRNPs@Pl and d) IRNPs@Ja after CV adsorption

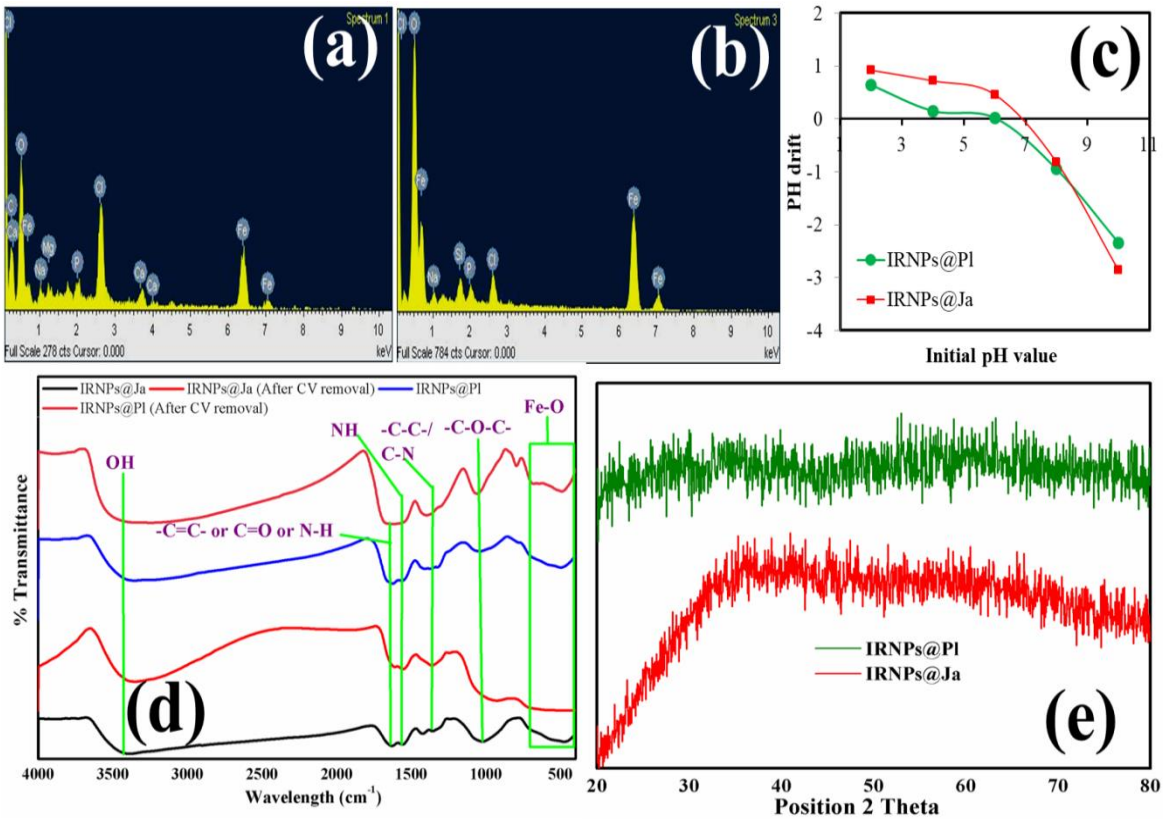

Fig. 2 EDS analysis of a) IRNPs@Pl and b) IRNPs@Ja, c) FTIR analysis and d) XRD analysis of IRNPs@Pl and IRNPs@Ja

EDS analysis of iron nanoparticles shows the presence of Fe, O, C and Cl as main elements of them (Fig. 2a and 2b). Iron nanoparticles immediately after synthesis may get oxidised in oxidative environment, therefore formation of iron oxide

on the surface of nanoparticles may take place. Presence of "Cl" might occur due to improper washing and presence of "C" shows the coated phytochemicals of the leaf extracts over the nanoparticles. The pH_{ZPC} of IRNPs@Pl and IRNPs@Ja was found to be 6.03 and 6.85, respectively and the graph for pH_{ZPC} has been shown in Fig. 2c. Similar functional groups were visible on the surfaces of both adsorbents in FTIR examination following their synthesis and application for adsorption (Fig. 2d). Main functional group that were identified were –OH, -NH, -C-C-, -CN, -C-O-C-, -C=C- and -C=O. A broad peak that appeared near 500 cm^{-1} represents the stretching of bond between metal and oxygen depicting the occurrence of Fe-O bond (Karpagavinayagam and Vedhi, 2019). The XRD analysis of both the nanoparticles lacked defined sharp peaks (Fig. 2e) that denotes the amorphous nature of the particles. In previous studies, other researchers also observed the green synthesis of iron nanoparticles with amorphous nature (Beheshtkhoo et al., 2018; Yi et al., 2019).

3.2. Study of CV adsorption

3.2.1. Effect of adsorbents concentration

The increment in the concentration of adsorbent was up to 2.5 g/L to remove 10 mg/L concentration of CV, at neutral pH and 25˚C. As Fig. 3a depicts the adsorption % of CV increased from 58 % to 87 % when the increment in concentration of IRNPs@Pl was done upto 1.0 g/L, whereas, adsorption percentage was increased from 53 % to 86 % on increasing the concentration of IRNPs@Ja upto 1.5 g/L. Furthermore increment in concentration of adsorbents resulted in decrease of adsorption. Percentage of adsorption significantly depends on the concentration of adsorbents as it determines the active sites for the adsorption. Therefore, CV adsorption was increased when concentration of IRNPs@Pl and IRNPs@Ja increased upto 1 and 1.5 g/L, respectively (Igwegbe et al., 2019). However, nanoparticles tend to get agglomerate at higher concentration which causes increase in their particle size, overlapping of active adsorption sites and sedimentation, which consequently decreases the adsorption (Mittal et al., 2020; Verma and Singh, 2022). Fig. 2a also depicts a decrease in q_t value (adsorption capacity) of both the adsorbents as their concentration was increased for adsorption, similar observation for q_t value was also reported by (Vidovix et al., 2022) that may occur due to saturation of active site. About 1 g/L and 1.5 g/L concentration of IRNPs@Pl and IRNPs@Ja, respectively, was used as optimum concentration for further adsorption study.

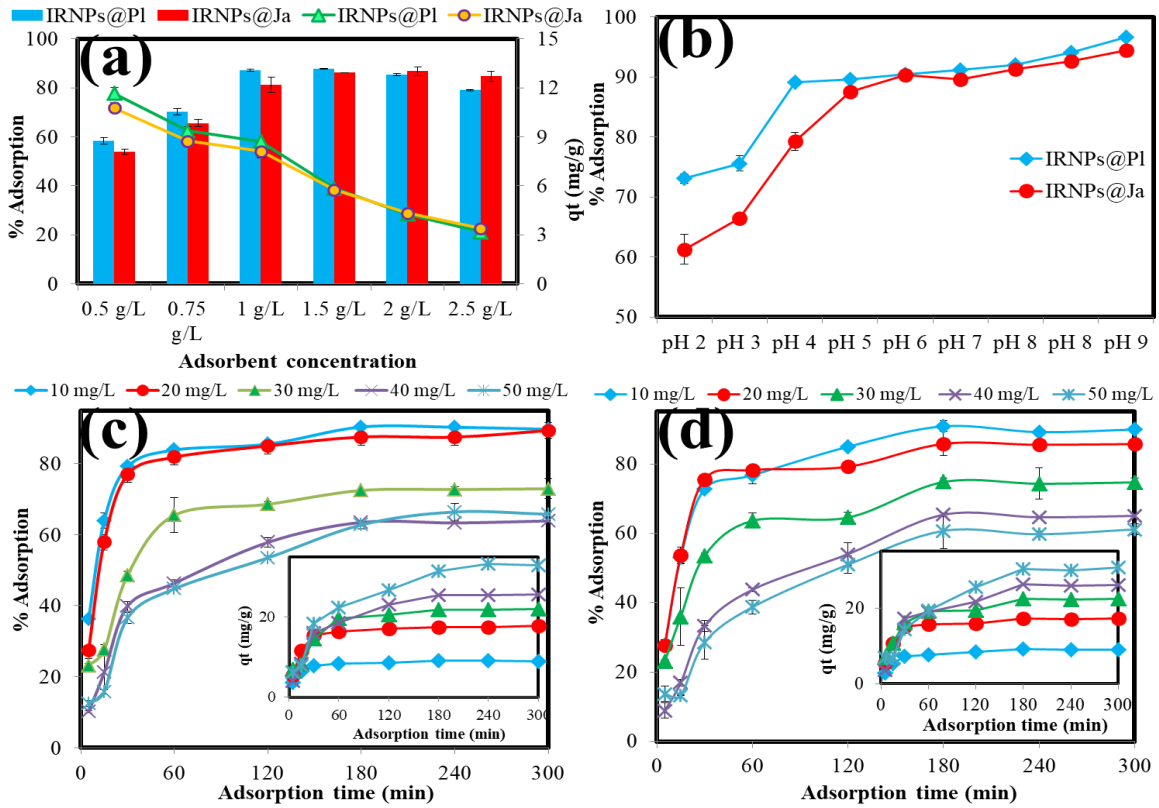

Fig. 3 Demonstration of a) adsorbent concentration effect, b) pH effect, and initial CV concentration effect on adsorption using c) IRNPs@Pl and d) IRNPs@Ja (inset graphs shows q_t values of adsorbents)

3.2.2. Effect of pH

Understanding the effects of pH on adsorption is crucial because it controls surface charge of the adsorbents and how the adsorbate is ionised (Uddin and Baig, 2019). The adsorption of CV was noticed to increase in higher pH. CV adsorption was increased from 73.05% to 96.62 % by IRNPs@Pl and from 61.95 % to 94.39 % by IRNPs@Ja on increasing pH 2 to 9 (Fig. 3b). CV is a basic dye which is

positively charged and at basic pH, the adsorbents acquires negative charge that attracts the oppositely charged dye molecule more. Hence the CV adsorption was increased at higher pH using both the adsorbents. Prajapati and Mondal (2020) also similarly reported an increase in adsorption of cationic dye (methylene blue) at basic pH.

3.2.3. Effect of CV concentration and adsorption time

CV concentration was enhanced up to 50 mg/L, whose outcomes have been shown in the Fig. 3c and 3d. The increase in concentration of CV resulted in the decrease of adsorption percentage from 85.50 % to 65.7 % using IRNPs@Pl and 89.91 % to 61.1 % using IRNPs@Ja. An increment in pollutant concentration, with constant concentration of adsorbent causes the available pollutant molecules to surpass the active adsorption sites responsible for adsorption. The remaining un-adsorbed dye in the solution decreases the adsorption percentage (Deb et al., 2019; Joshi et al., 2019). The inset graphs show the variation in q_t value at different concentration of CV which shows that the value of q_t was increased with an increasing the CV concentration. Maximum q_t of IRNPs@Pl was 32.8 mg/g and that of IRNPs@Ja was found 30.5 mg/g at 50 mg/L. The higher value of q_t at higher CV concentration may result from the higher mass transfer driving force (Reghioua et al., 2021; Singh et al., 2019).

An impact of adsorption time on CV adsorption were studied along with the above study. Adsorption was rapid and significant using both the adsorbents in initial 60 min after that the removal percentages were found lesser and slower (Fig. 2c and 2d). In initial stage of adsorption, all the active adsorption sites are vacant which allows a large amount of dye to get adsorbed; therefore, in the starting of process the adsorption was fast. As most of the active sites get covered by dye molecules the adsorption slows down due to low driving force towards adsorbents and an equilibrium state was achieved at around 180 min (Liu et al., 2019; Mansour et al., 2022a).

3.2.4. Effect of temperature

As the Fig. 4a and 4b shows the adsorption of CV was increasing with an increase in operating temperature using both the adsorbents. The increasing adsorption trend represents an endothermic adsorption reaction. Previous literature also reports endothermic adsorption of dye over iron nanoparticles (Wang et al., 2021).

3.3. Adsorption isotherm, kinetics and thermodynamics

Plots for all the adsorption isotherms have been represented in Fig. 4c to 4e, and table 2 gives the values of their different parameters along with their respective R^2. On comparing R^2 value for all isotherms the adsorption of CV using IRNPs@Pl was found followed best by Langmuir isotherm (R^2= 0.963), while adsorption using IRNPs@Ja was best followed by Temkin isotherm (R^2= 0.990). The maximum adsorption capacity (Q_0) of IRNPs@Pl and IRNPs@Ja was 33.55 mg/g.

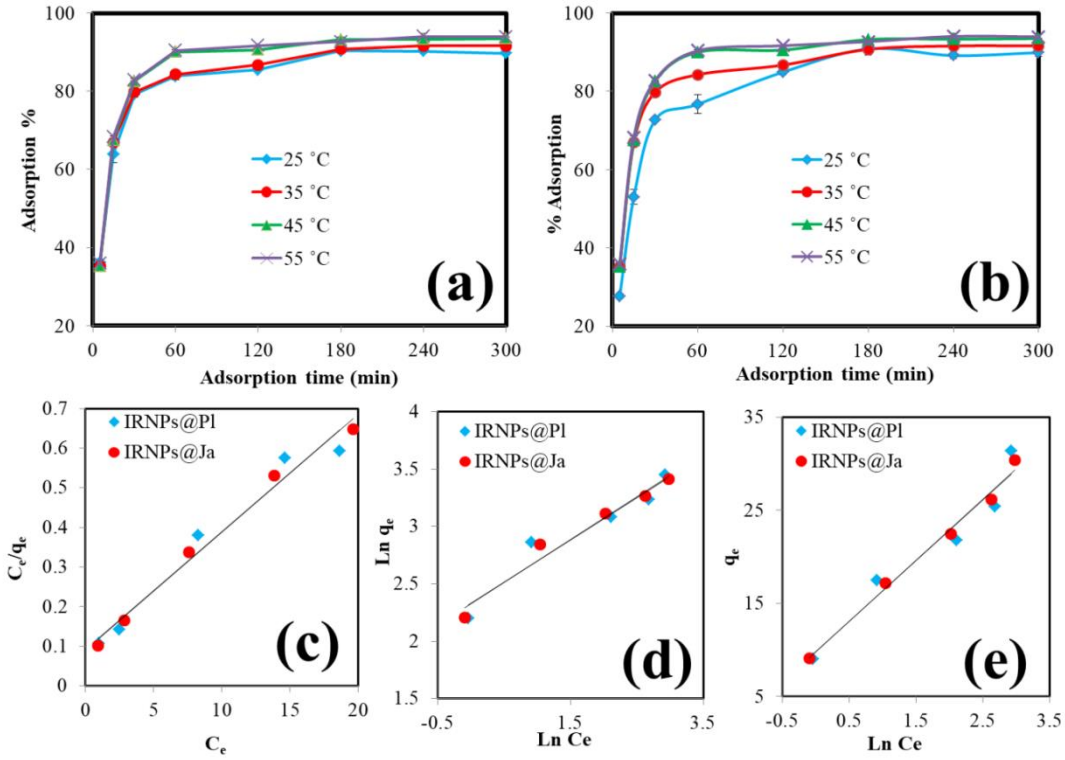

Fig. 4 Demonstration of temperature effect on adsorption of CV using a) IRNPs@Pl and b) IRNPs@Ja and c), d) and e) plot of Langmuir, Freundlich and Temkin isotherm, respectively.

Table 2 Values of adsorption isotherm parameters for CV adsorption

	Langmuir Isotherm		Freundlich Isotherm		Temkin Isotherm	
	Parameters	**Values**	**Parameters**	**Values**	**Parameters**	**Values**
IRNPs@Pl	**Q_0 (mg/g)**	33.557± 1.2	**K_F (mg/g(L/mg)$^{1/n}$)**	10.285±0.8	**B**	6.525±0.3
	b (L/mg)	0.002± 0.0003	**n**	2.712±0.2	**A (L/g)**	4.482±0.01
	R_L	0.973±0.05	**R^2**	0.932±0.05	**R^2**	0.941±0.003
	R^2	0.963±0.05				
IRNPs@Ja	**Q_0 (mg/g)**	33.557± 1.2	**K_F (mg/g(L/mg)$^{1/n}$)**	2.668±0.05	**B**	6.587±0.08
	b (L/mg)	0.002±0.0003	**n**	10.209±0.3	**A (L/g)**	4.370±0.6
	R_L	0.974±0.04	**R^2**	0.970±0.02	**R^2**	0.990±0.05
	R^2	0.989±0.02				

Fig. 5a to 5f shows the plots for pseudo-first-order kinetic, pseudo-second-order kinetic and intraparticle diffusion model and values of their respective parameters and R^2 is provided in Table 3. The CV adsorption data of IRNPs@Pl and IRNPs@Ja was found to fitted best with Pseudo-second-order kinetics.

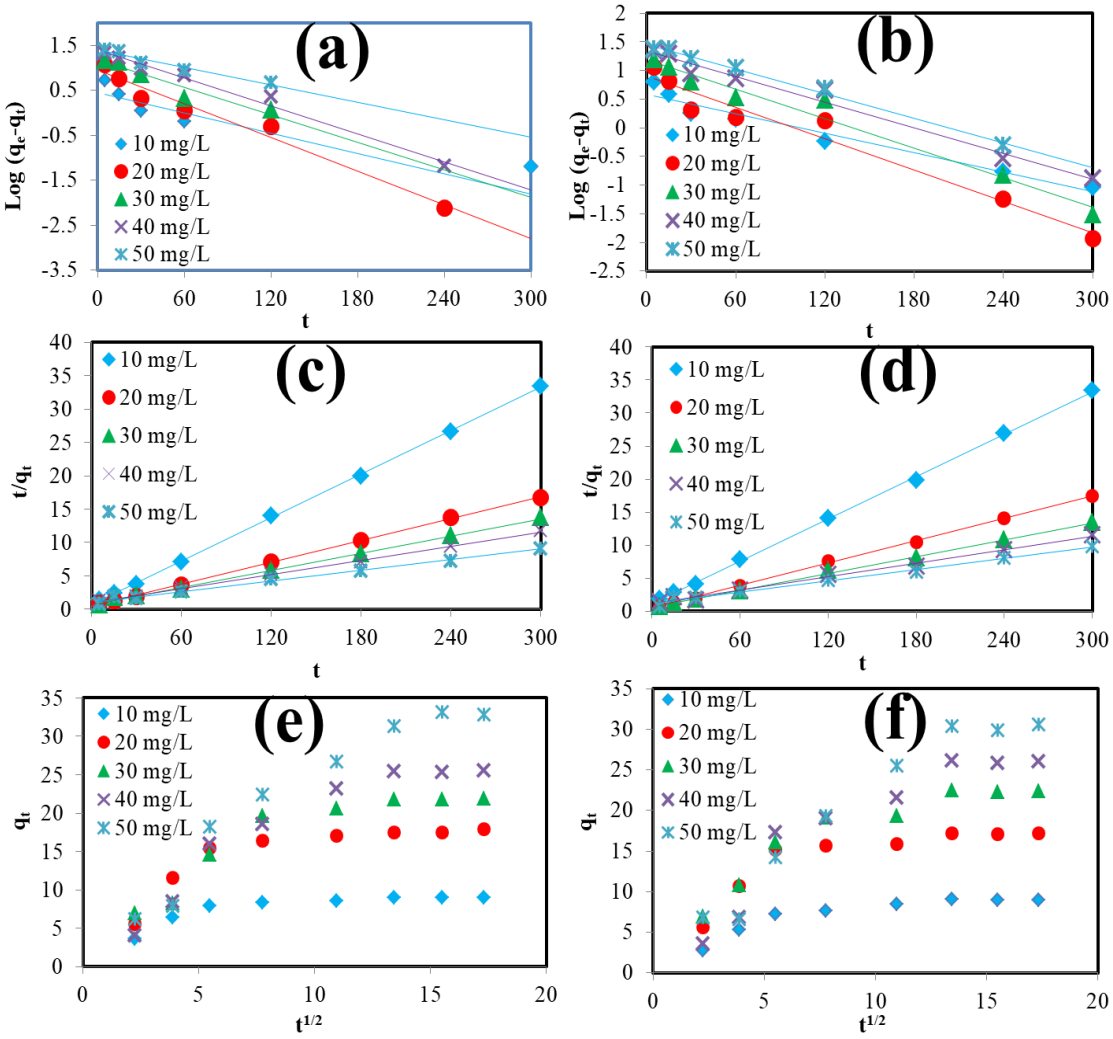

Fig. 5 Pseudo-first-order kinetics plots for a) IRNPs@Pl and b) IRNPs@Ja, pseudo-second-order kinetics plots for c) IRNPs@Pl and d) IRNPs@Ja, intraparticle diffusion model plots for e) IRNPs@Pl and f) IRNPs@Ja

The regression line did not cross the origin in the intraparticle diffusion model plot, indicating that the adsorption process was not primarily caused by the intraparticle diffusion model.

Table 3 Values of kinetics parameters for CV adsorption

		Pseudo first order kinetics			Pseudo second order		
	C_0 (mg/L)	q_e (mg/g)	k_1 (min^{-1})	R^2	q_e (mg/g)	k_2 (g/mg min))	R^2
IRNPs@Pl	10	2.836612	0.003257	0.7993	9.21659	0.016825	0.9997
	20	8.910457	0.005428	0.9707	18.28154	0.006381	0.9997
	30	15.03142	0.004429	0.912	23.31002	0.002556	0.9978
	40	25.30463	0.004516	0.985	28.40909	0.001204	0.9981
	50	25.02649	0.002779	0.95	37.59398	0.000675	0.9915
IRNPs@Ja	10	3.88508	0.002475	0.9557	9.363296	0.009743	0.9995
	20	8.061206	0.003951	0.9596	17.69912	0.006293	0.9993
	30	15.67112	0.003734	0.9734	23.64066	0.002711	0.998
	40	22.29462	0.003257	0.981	29.5858	0.000944	0.9921
	50	28.64178	0.003126	0.9928	35.46099	0.000645	0.9861

Plot for thermodynamics has been shown in Fig 6a and values of ΔH˚, ΔS˚ and ΔG˚ have been provided in Table 3. The positive ΔH˚ value for both the adsorbents represents endothermic adsorption of CV and negative ΔG˚ value represents the spontaneous behaviour of the reaction.

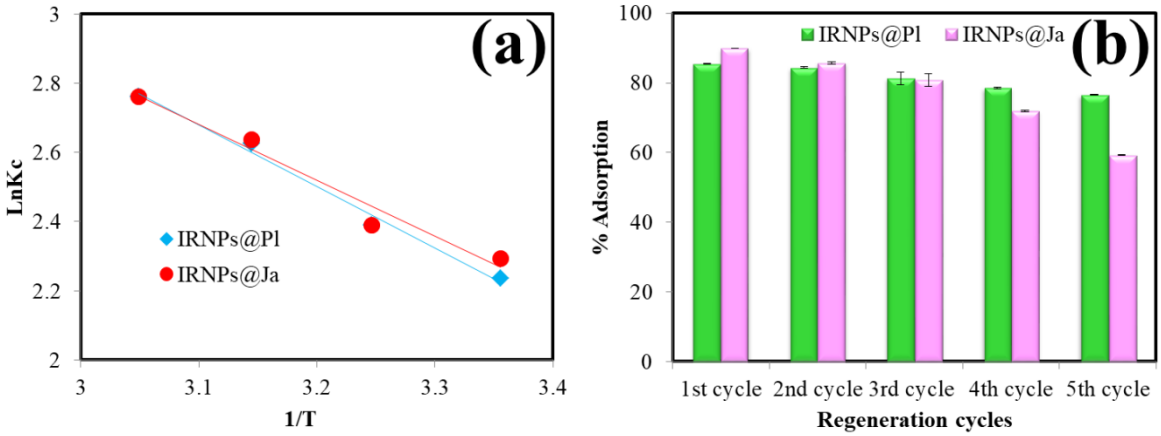

Fig. 6 a) Thermodynamics plot, b) regeneration of adsorbents

Table 4 Parameters of thermodynamic

	Temperature (K)	ΔG˚ (KJ/mol)	ΔH˚ (KJ/mol)	ΔS˚ (KJ/mol K)
IRNPs@Pl	**298**	-20.2362± 0.3	0.0133±00.01	0.0679±0.002
	308	-20.9158±0.6		
	318	-21.5953±1.5		
	328	-22.2749±0.6		
IRNPs@Ja	**298**	-18.9958± 1.3	0.0133±00.01	0.0637±0.009
	308	-19.6337±0.6		
	318	-20.2716±0.9		
	328	-20.9095±0.02		

3.4. Regeneration of adsorbents

Recycling of the adsorbents decreases their adsorption efficiency to some extents as depicted in Fig. 6b. The adsorption percentage of CV using IRNPs@Pl decreased from 85.50 % to 76.58 %, and by using IRNPs@Ja, the adsorption percentage was reduced from 89.91 % to 59.34 % in the fifth cycle. During recycling, some amount of adsorbent may get lost due to the process of washing which can reduce the adsorption efficiency (Mansour et al., 2022b; Rawat and Singh, 2022). Furthermore, some of the adsorption sites may get denature or get covered by pollutant resulting in a decrease in adsorption efficiency.

4. Conclusion

A successful conversion of an iron waste such as iron rust into valuable iron nanoparticles, iron rust is commonly produced by the corrosion of iron utilities. These nanoparticles had good efficiency for the adsorption of CV

from water. Adsorption capacity of both the nanoparticles (Q_0) was found to be 33.5 mg/g. The adsorption process was endothermic and it was favoured by higher pH. The nanoparticles were successfully recycled for five cycles; however, during the process of recycling the adsorption efficiency of IRNPs@Pl was better in comparison with IRNPs@Ja. Synthesis of nanoparticles using waste makes the process less costly. A utilization of plant extracts in green synthesis of nanoparticles, further reduces the cost of synthesis of nanomaterials and made it environmental friendly process.

Conflict of interest

Author declares no conflict of interest.

Contribution of authors

Shalu Rawat (Ph.D. student) conducted all experiments and drafted manuscript and Dr. **Jiwan Singh (Assistant Professor)** has supervised the work, edited and reviewed the manuscript.

Acknowledgement

Authors thankfully acknowledge the financial support by University Grant Commission (UGC-BSR Research start up grant: project no. F. 30-382/2017, BSR) and Science and Engineering Research Board-Department of Science and Technology (SERB-DST), India (project No. ECR/2016/001924) for this work. Authors also acknowledge the funding in the form of Junior Research Fellowship (UGC-Ref. No: 3840/(NET-DEC 2018) to the first author by University Grant Commission (UGC), New Delhi.

References

Abdulhameed, A.S., Jawad, A.H., Mohammad, A.T., 2019. Synthesis of chitosan-ethylene glycol diglycidyl ether/TiO2 nanoparticles for adsorption of reactive orange 16 dye using a response surface methodology approach. Biores. Technol. 293, 122071.

Akintelu, S.A., Folorunso, A.S., Folorunso, F.A., Oyebamiji, A.K., 2020. Green synthesis of copper oxide nanoparticles for biomedical application and environmental remediation. Heliyon. 6(7), e04508.

Badeenezhad, A., Azhdarpoor, A., Bahrami, S., Yousefinejad, S., 2019. Removal of methylene blue dye from aqueous solutions by natural clinoptilolite and clinoptilolite modified by iron oxide nanoparticles. Mol. Simul. 45(7), 564-571.

Beheshtkhoo, N., Kouhbanani, M.A.J., Savardashtaki, A., Amani, A.M., Taghizadeh, S., 2018. Green synthesis of iron oxide nanoparticles by aqueous leaf extract of Daphne mezereum as a novel dye removing material. Appl. Phys. A. 124(5), 1-7.

Bhan, C., Singh, J., 2022. Fabrication of an adsorbent from Ficus racemosa leaf biomass for fluoride removal and its preparation cost analysis. J. Appl. Sci. Innov. Technol. 1(1), 1-5.

Chatterjee, S., Guha, N., Krishnan, S., Singh, A.K., Mathur, P., Rai, D.K., 2020. Selective and recyclable Congo red dye adsorption by spherical Fe_3O_4 nanoparticles functionalized with 1, 2, 4, 5-benzenetetracarboxylic acid. Sci. Rep. 10(1), 1-11.

Chowdhury, A., Kumari, S., Khan, A.A., Chandra, M.R., Hussain, S., 2021. Activated carbon loaded with Ni-Co-S nanoparticle for superior adsorption capacity of antibiotics and dye from wastewater: kinetics and isotherms. Colloids Surf A. 611, 125868.

Das, A., Kamle, M., Bharti, A., Kumar, P., 2019. Nanotechnology and it's applications in environmental remediation: an overview. Vegetos. 32(3), 227-237.

Deb, A., Kanmani, M., Debnath, A., Bhowmik, K.L., Saha, B., 2019. Ultrasonic assisted enhanced adsorption of methyl orange dye onto polyaniline impregnated zinc oxide nanoparticles: kinetic, isotherm and optimization of process parameters. Ultrason. Sonochem. 54, 290-301.

Elgarahy, A.M., Elwakeel, K.Z., Akhdhar, A., Hamza, M.F., 2021. Recent advances in greenly synthesized nanoengineered materials for water/wastewater remediation: an overview. Nanotechnol. Environ. Eng. 6(1), 1-24.

Hao, R., Li, D., Zhang, J., Jiao, T., 2021. Green synthesis of iron nanoparticles using green tea and its removal of hexavalent chromium. Nanomaterials 11(3), 650.

Igwegbe, C.A., Mohmmadi, L., Ahmadi, S., Rahdar, A., Khadkhodaiy, D., Dehghani, R., Rahdar, S., 2019. Modeling of adsorption of methylene blue dye on Ho-CaWO4 nanoparticles using response surface methodology (RSM) and artificial neural network (ANN) techniques. MethodsX. 6, 1779-1797.

Joshi, S., Garg, V.K., Kataria, N., Kadirvelu, K., 2019. Applications of Fe3O4@ AC nanoparticles for dye removal from simulated wastewater. Chemosphere. 236, 124280.

Karpagavinayagam, P., Vedhi, C., 2019. Green synthesis of iron oxide nanoparticles using Avicennia marina flower extract. Vacuum. 160, 286-292.

Kaur, K., Sidhu, A.K., 2021. Green synthesis: An eco-friendly route for the synthesis of iron oxide nanoparticles. Front. Nanotechnol. 3, 655062.

Khan, S., Naushad, M., Al-Gheethi, A., Iqbal, J., 2021. Engineered nanoparticles for removal of pollutants from wastewater: Current status and future prospects of nanotechnology for remediation strategies. J. Environ. Chem. Eng. 9(5), 106160.

Khani, R., Roostaei, B., Bagherzade, G., Moudi, M., 2018. Green synthesis of copper nanoparticles by fruit extract of Ziziphus spina-christi (L.) Willd.: application for adsorption of triphenylmethane dye and antibacterial assay. J. Mol. Liq. 255, 541-549.

Kumar, S., et al. 2020. Nanoscale zinc oxide based heterojunctions as visible light active photocatalysts for hydrogen energy and environmental remediation. Catal. Rev. 62.3, 346-405.

Leonel, A.G., Mansur, A.A., Mansur, H.S., 2021. Advanced functional nanostructures based on magnetic iron oxide nanomaterials for water remediation: a review. Water Res. 190, 116693.

Linley, S., Thomson, N.R., 2021. Environmental applications of nanotechnology: nano-enabled remediation processes in water, soil and air treatment. Water Air Soil Pollut. 232(2), 1-50.

Liu, J., Wang, N., Zhang, H., Baeyens, J., 2019. Adsorption of Congo red dye on FexCo3-xO4 nanoparticles. J. Environ. Manage. 238, 473-483.

Mansour, A.T., Alprol, A.E., Abualnaja, K.M., El-Beltagi, H.S., Ramadan, K.M., Ashour, M., 2022b. The Using of Nanoparticles of Microalgae in Remediation of Toxic Dye from Industrial Wastewater: Kinetic and Isotherm Studies. Materials. 15(11), 3922.

Mansour, A.T., Alprol, A.E., Khedawy, M., Abualnaja, K.M., Shalaby, T.A., Rayan, G., Ashour, M., 2022a. Green synthesis of zinc oxide nanoparticles using red seaweed for the elimination of organic toxic dye from an aqueous solution. Materials. 15(15), 5169.

Mashkoor, F., Nasar, A., 2020. Magnetized *Tectona grandis* sawdust as a novel adsorbent: preparation, characterization, and utilization for the removal of methylene blue from aqueous solution. Cellulose 27(5), 2613-2635.

Mishra, B., Kumar, A., Tripathi, B.P., 2020. Polydopamine mediated in situ synthesis of highly dispersed Gold nanoparticles for continuous flow catalysis and environmental remediation. J. Environ. Chem. Eng. 8(5), 104397.

Mittal, H., Morajkar, P.P., Al Alili, A., Alhassan, S.M., 2020. In-situ synthesis of ZnO nanoparticles using gum arabic based hydrogels as a self-template for effective malachite green dye adsorption. J. Polym. Environ. 28(6), 1637-1653.

Nazir, G., Rehman, A., Park, S.J., 2021. Valorization of shrimp shell biowaste for environmental remediation: Efficient contender for CO_2 adsorption and separation. J. Environ. Manage. 299, 113661.

Parmar, A., Kaur, G., Kapil, S., Sharma, V., Choudhary, M.K., Sharma, S., 2019. Novel biogenic silver nanoparticles as invigorated catalytic and antibacterial tool: a cleaner approach towards environmental remediation and combating bacterial invasion. Mater. Chem. Phys. 238, 121861.

Pasinszki, T., Krebsz, M., 2020. Synthesis and application of zero-valent iron nanoparticles in water treatment, environmental remediation, catalysis, and their biological effects. Nanomaterials 10(5), 917.

Prajapati, A.K., Mondal, M.K., 2020. Comprehensive kinetic and mass transfer modeling for methylene blue dye adsorption onto CuO nanoparticles loaded on nanoporous activated carbon prepared from waste coconut shell. J. Mol. Liq. 307, 112949.

Qian, Y., Qin, C., Chen, M., Lin, S., 2020. Nanotechnology in soil remediation− applications vs. implications. Ecotoxicol. Environ. Saf. 201, 110815.

Rawat, S., Singh, J., 2021. Green synthesis of iron nanoparticles using Plumeria and Jatropha: Characterization and investigation of their adsorption, regeneration and catalytic degradation efficiencies. BioNanoScience 11(4), 1142-1153.

Rawat, S., Singh, J., 2022. Degradation of paranitrophenol by green synthesised iron nanoparticles: Optimization of the process parameters and study of degradation kinetics. J. Appl. Sci. Innov. Technol. 1(1), 21-26.

Rawat, S., Singh, J., 2023. Fenton like oxidative degradation of toxic water pollutants by iron nanoparticles synthesized via facile green route using waste iron rust as the iron precursor. Environ. Eng. Res. 28(2).

Reghioua, A., Barkat, D., Jawad, A.H., Abdulhameed, A.S., Khan, M.R., 2021. Synthesis of Schiff's base magnetic crosslinked chitosan-glyoxal/ZnO/Fe3O4 nanoparticles for enhanced adsorption of organic dye: modeling and mechanism study. Sustain. Chem. Pharm. 20, 100379.

Saruchi., Thakur, P., Kumar, V., 2019. Kinetics and thermodynamic studies for removal of methylene blue dye by biosynthesize copper oxide nanoparticles and its antibacterial activity. J. Environ. Health Sci. Eng. 17(1), 367-376.

Sharma, S., Hasan, A., Kumar, N., Pandey, L.M., 2018. Removal of methylene blue dye from aqueous solution using immobilized Agrobacterium fabrum biomass along with iron oxide nanoparticles as biosorbent. Environ. Sci. Pollut. Res. 25(22), 21605-21615.

Shukla, K., Verma, A., Verma, L., Rawat, S., Singh, J., 2020. A novel approach to utilize used disposable paper cups for the development of adsorbent and its application for the malachite green and rhodamine-B dyes removal from aqueous solutions. Nat. Environ. Pollut. Technol. 19(1), 57-70.

Singh, J., Reddy, K.J., Chang, Y.Y., Kang, S.H., Yang, J.K., 2016. A novel reutilization method for automobile shredder residue as an adsorbent for the removal of methylene blue: Mechanisms and heavy metal recovery using an ultrasonically assisted acid. Process Saf. Environ. Prot. 99, 88-97.

Singh, N., Riyajuddin, S., Ghosh, K., Mehta, S.K., Dan, A., 2019. Chitosan-graphene oxide hydrogels with embedded magnetic iron oxide nanoparticles for dye removal. ACS Appl. Nano Mater. 2(11), 7379-7392.

Uddin, M.K., Baig, U., 2019. Synthesis of Co3O4 nanoparticles and their performance towards methyl orange dye removal: Characterisation, adsorption and response surface methodology. J. Clean. Prod. 211, 1141-1153.

Verma, L., Singh, J., 2022. As(III) removal using engineered biochar synthesized from waste biomass of a Timber plant refuse. J. Appl. Sci. Innov. Technol. 1(1), 6-9.

Vidovix, T.B., Quesada, H.B., Bergamasco, R., Vieira, M.F., Vieira, A.M.S., 2022. Adsorption of Safranin-O dye by copper oxide nanoparticles synthesized from Punica granatum leaf extract. Environ. Technol. 43(20), 3047-3063.

Wang, X., Zhang, Y., Shan, R., Hu, H., 2021. Polydopamine interface encapsulating graphene and immobilizing ultra-small, active Fe_3O_4 nanoparticles for organic dye adsorption. Ceram. Int. 47(3), 3219-3231.

Wang, Y., Pan, C., Chu, W., Vipin, A.K., Sun, L., 2019. Environmental remediation applications of carbon nanotubes and graphene oxide: Adsorption and catalysis. Nanomaterials 9(3), 439.

Xiao, C., Li, H., Zhao, Y., Zhang, X., Wang, X., 2020. Green synthesis of iron nanoparticle by tea extract (polyphenols) and its selective removal of cationic dyes. J. Environ. Manage. 275, 111262.

Yi, Y., Tu, G., Tsang, P.E., Xiao, S., Fang, Z., 2019. Green synthesis of iron-based nanoparticles from extracts of Nephrolepis auriculata and applications for Cr (VI) removal. Mater. Lett. 234, 388-391.

Zhang, W., Zhang, D., Liang, Y., 2019. Nanotechnology in remediation of water contaminated by poly-and perfluoroalkyl substances: a review. Environ. Pollut. 247, 266-276.

Cite this article:

Rawat, S., Singh, J., 2022. Fabrication of iron nanoparticles by reusing an iron waste and their application as efficient adsorbents to remove crystal violet dye from water. J.Appl. Sci. Innov. Technol. 1 (2), 37-46